JOURNAL OF THERMOPHYSICS AND HEAT TRANSFER
Vol. 21, No. 3, July–September 2007

Spectroscopic Diagnostics of Thermochemical Nonequilibrium Hydrogen Plasma Flow

Yoshiki Takama* and Kojiro Suzuki†
University of Tokyo, Chiba 277-8561, Japan

DOI: 10.2514/1.28288

A method to diagnose thermochemical nonequilibrium hydrogen plasma flow nonintrusively by emission spectroscopy has been developed. The rotational, vibrational, and electron temperatures have been obtained by the preprocessed line intensity fitting of Fulcher-α band of molecular hydrogen, and the degree of dissociation by the actinometry. In the preprocessed line intensity fitting, the temperatures are guessed on the basis of the similarity of Boltzmann distribution to make the searching domain smaller. As a result, it has become possible to identify the plasma temperatures more easily. Then our method has been applied to the inductively coupled plasma wind tunnel to determine the freestream conditions. The obtained total enthalpy, which is composed of the internal energy, kinetic energy, and chemical energy, shows a reasonable tendency to be almost inversely proportional to the mass flow rate under the condition of fixed input power. The possible error in the temperatures, the degree of dissociation, and the total enthalpy is evaluated in the component-by-component manner.

Nomenclature

A	=	transition probability
C	=	excitation rate coefficient
E_{thre}	=	threshold energy
F	=	rotational energy
G	=	vibrational energy
h	=	Pranck constant
I	=	emission intensity
J	=	rotational quantum number
k	=	Boltzmann constant
N	=	number density
n_e	=	electron number density
R_i	=	Gas constant of ith speices
T_e	=	electron temperature
T_{ele}	=	electronic excitation temperature
T_{rot}	=	rotational temperature
T_{tra}	=	translational temperature
T_{vib}	=	vibrational temperature
Y	=	mass fraction
v	=	vibrational quantum number
α	=	degree of dissociation
ν	=	frequency

I. Introduction

CONTINUOUS explorations of outer planets are expected in the future, because they will give us a lot of knowledge and discoveries in planetary science like the Galileo mission. In the cases of those atmospheric entries, the spacecraft experience significant aerodynamic heating from the high-temperature shock layer flow, which is mainly composed of hydrogen plasma. Therefore, the accurate prediction of aerodynamic heating from hydrogen plasma is one of the most important problems to make those missions feasible. The high-enthalpy plasma wind tunnels are used for the simulation of those planetary entry environments and for the material heating tests. However, it is difficult to know the freestream condition of the wind tunnels such as plasma temperatures and chemical composition accurately. One of the reasons is that the method to measure those nonequilibrium quantities has not been established.

The Langmuir probe method is widely used in the measurement of the electron temperature. However, it is intrusive to the test flow. Because it requires only the electric current from the thermal motions of charged particles, it is difficult to distinguish between the current from the thermal motions and the total probe current in the case of the flowing plasma. When the flow is supersonic, the shock wave caused by the probe can completely change the flowfield and the chemical composition. In this case, the probe does not measure the electron temperature of the freestream anymore. Therefore, the Langmuir probe method is not appropriate for the exact plasma diagnostics for the high-enthalpy plasma wind tunnel.

In this work, we propose a nonintrusive diagnostic method of thermochemical nonequilibrium hydrogen plasma by emission spectroscopy. As the nonequilibrium quantities, we determine the rotational, vibrational, and electron temperatures by the spectral fitting of hydrogen molecular band and the degree of dissociation by the actinometry. In the usual spectral fitting of molecular band, there are so many line spectra to interfere with each other in the band that we have to take into account the effect of spectral broadening beforehand and to fit the whole band spectra. However in this work, we choose Fulcher-α band of hydrogen molecule, in which several lines have high intensity and they are not interfered with by other lines. The peak intensities can be identified and detected accurately by a spectrometer. Therefore, we use only their peak intensities in the spectral fitting, not the whole band spectra. We call this method *line intensity fitting*. The computation time for the line intensity fitting is much smaller than that for the usual spectral fitting. In the actinometry, we seed hydrogen plasma with a small amount of argon, and we determine the degree of dissociation from the intensity ratio of H 656.3 nm line to that of Ar 750.4 nm line. These two lines and Fulcher-α band do not interfere with each other. As a result, our nonintrusive method enables us to determine the plasma properties of hydrogen plasma easily and effectively. Finally, our nonintrusive diagnostics is applied to the inductively coupled plasma (ICP) wind tunnel to determine its freestream condition. From the calculation of the total enthalpy, we assess the validity of our method.

The objectives of this research are 1) to develop a nonintrusive diagnostic method of thermochemical nonequilibrium hydrogen

Presented as Paper 3819 at the 9th AIAA/ASME Joint Thermophysics and Heat Transfer Conference, San Francisco, 5–8 June 2006; received 10 October 2006; revision received 26 January 2007; accepted for publication 26 January 2007. Copyright © 2007 by the American Institute of Aeronautics and Astronautics, Inc. All rights reserved. Copies of this paper may be made for personal or internal use, on condition that the copier pay the $10.00 per-copy fee to the Copyright Clearance Center, Inc., 222 Rosewood Drive, Danvers, MA 01923; include the code 0887-8722/07 $10.00 in correspondence with the CCC.

*Graduate Student, JSPS Research Fellow, Department of Advanced Energy, 5-1-5, Kashiwanoha, Kashiwa; takama@daedalus.k.u-tokyo.ac.jp. Student Member AIAA.

†Associate Professor, Department of Advanced Energy, 5-1-5, Kashiwanoha, Kashiwa; kjsuzuki@k.u-tokyo.ac.jp. Member AIAA.

plasma and 2) to determine the freestream condition of the plasma wind tunnel by this method.

II. Preprocessed Line Intensity Fitting

For the measurement of the plasma temperatures, we propose the method called *preprocessed line intensity fitting*. We use the molecular spectra of Fulcher-α band of hydrogen molecule in this work. By using an appropriate radiation model based on quantum mechanics, the rotational, vibrational, and electron temperatures of hydrogen plasma can be determined. We add "preprocessing" before the line intensity fitting to improve the accuracy of the fitting. This section consists of four parts: First in Sec. II.A, the band system used in this work is explained. In Sec. II.B, the radiation model and the method to calculate the theoretical spectra are described. In Sec. II.C, the outline of the preprocessed line intensity fitting is explained. In Sec. II.D, the preprocessing we have introduced in this work is described. The error evaluation is shown in Sec. V.D.1.

A. Fulcher-α Band

In hydrogen plasma, Fulcher-α band spectra are appropriate for the measurement and often used [1–3] because they are in the visible range (590–640 nm) and relatively free from the interferences by other emission lines.

The term diagram of hydrogen molecule is shown in Fig. 1, illustrating the excitation mechanism for the band in the Fulcher-α system [4]. For each rotational state, parity $(+,-)$ and symmetry property (s,a) are shown. Each transition obeys the selection rules for ΔJ, parity, and symmetry property [5]. The emission occurs when the molecule transits from Fulcher upper state $d^3\Pi_u$ to Fulcher lower state $a^3\Sigma_g^+$ after being excited from the ground state $X^1\Sigma_g^+$ to the upper state. Physical quantities of the ground state are denoted by no primes, those of Fulcher upper state by single prime, and those of Fulcher lower state by double primes. The state $d^3\Pi_u$ degenerates into the $d^3\Pi_u^-$ and $d^3\Pi_u^+$ states. The selection rule requires that the former can have only Q branch, and the latter both P and R branches. Among three branches, the lines of Q branch (no change in rotational quantum number) are the most suitable for spectroscopy. This is because the strong interaction between the state $d^3\Pi_u^+$ and the state $e^3\Sigma_g^+$ makes P and R branches perturbed [6]. Therefore, the following discussion is restricted to Q branch.

B. Calculation of Theoretical Spectra

Emission intensity is described as follows:

$$I_{v'',J''}^{v',J'} = h\nu_{v'',J''}^{v',J'} N_{v',J'} A_{v'',J''}^{v',J'} \tag{1}$$

Assuming Born–Oppenheimer approximation and Franck–Condon principle, the transition probability is given by [5]

$$A_{v'',J''}^{v',J'} = \frac{64\pi^4 \left(\nu_{v'',J''}^{v',J'}\right)^3}{3h(2J'+1)} q_{v',v''} S_{J',J''} R_e^2 \tag{2}$$

where R_e^2 is the average value of the electronic transition moment,

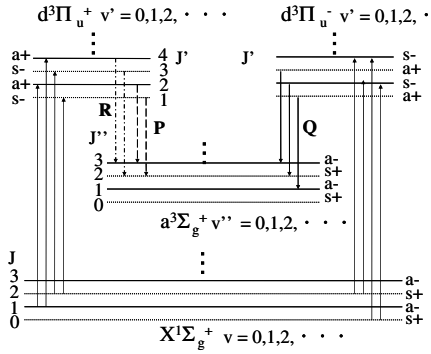

Fig. 1 Fulcher-α band system.

and is assumed to be constant. $q_{v',v''}$ is the Franck–Condon factor [7]. $S_{J',J''}$ is the Hönl–London factor, which is $(2J'+1)/2$ in the case of Q branch.

Assuming corona equilibrium, in which the excitation path is only electron impact from the ground state and the deexcitation path is only radiation to Fulcher lower state, the population at Fulcher upper state is described by

$$n_e \sum_{v,J} N_{v,J} C_{v,J}^{v',J'} = N_{v',J'} \sum_{v'',J''} A_{v'',J''}^{v',J'} \tag{3}$$

The preceding equation means that the stepwise excitation through the metastable states, the cascading from the upper states than Fulcher upper state, the quenching by collisions, and the predissociation are neglected. The possible error by this assumption is evaluated in Sec. V.D.2.

Then the rate coefficient from the ground state to Fulcher upper state is estimated. By the selection rule, only the transition satisfying that $J'-J$ is even is allowed. The rate coefficient consists of three components by rotational, vibrational, and electron energy: 1) contribution by rotational energy: proportional to the rotational branching ratio shown by Winger3j-symbol [8,9], 2) contribution by vibrational energy: proportional to Franck–Condon factor [1], and 3) contribution by electron energy: proportional to Arrhenius-type dependence [2].

Then the rate coefficient is estimated by

$$C_{v,J}^{v',J'} \propto (2J'+1)\begin{pmatrix} J' & 1 & J \\ 1 & -1 & 0 \end{pmatrix}^2 q_{v,v'} \exp\left(-\frac{\Delta E}{kT_e}\right) \quad (J'-J \text{ is even})$$
$$C_{v,J}^{v',J'} = 0 \quad (J'-J \text{ is odd}) \tag{4}$$

where the second bracket in Eq. (4) denotes Wigner3j-symbol. It is zero except the case that $J'-J=0,\pm1$. Considering the selection rule, it means that we assume that the rotational quantum number is unchanged in the transition from the ground state to Fulcher upper state.

Assuming the Boltzmann distribution at the ground state, the population at (v,J) state is described as

$$N_{v,J} \propto (2J+1) g_J \exp\left(-\frac{F(v,J)}{kT_{\text{rot}}} - \frac{G(v)}{kT_{\text{vib}}}\right) \tag{5}$$

Note that the rotational energy is also a function of the vibrational quantum number v due to the coupling of rotation and vibration. The rotational and vibrational energies are described as follows:

$$F(v,J) = B_v J(J+1) - D_v J^2 (J+1)^2 \tag{6}$$

$$G(v) = \omega_e\left(v+\frac{1}{2}\right) - \omega_e x_e \left(v+\frac{1}{2}\right)^2 \tag{7}$$

$$B_v = B_e - \alpha_e\left(v+\frac{1}{2}\right) \tag{8}$$

$$D_v = D_e + \beta_e\left(v+\frac{1}{2}\right) \tag{9}$$

where B_e, D_e, α_e, β_e, ω_e, and $\omega_e x_e$ are rotational and vibrational constants for the electronic states [5]. g_J is the degeneracy to describe the nuclear spin of homonuclear diatomic molecule. It is 3 for odd J, and 1 for even J in the case of H_2.

Using Eqs. (1) and (3–5), the theoretical emission intensities of Fulcher-α band can be calculated as a function of three temperatures: T_{rot}, T_{vib}, and T_e.

Table 1 Selected spectral lines, nm

Transition (v'-v'')	$Q1$	$Q2$	$Q3$
0-0	601.83	602.38	603.19
1-1	612.18	–	613.54
2-2	622.48	623.03	623.84

C. Outline of Preprocessed Line Intensity Fitting

Plasma temperatures are determined by the line intensity fitting. The method is to identify the temperatures by which the calculated spectra reproduce the experimental data with the best accuracy. Several spectral lines of Fulcher-α band are selected, and the peak intensities of their emissions are compared with the calculated spectra. The spectra width is not taken into account in this work. The measurement accuracy of the peak intensity is mentioned in Sec. V. D.1.

Eight lines used here are chosen from the viewpoints of 1) high emission intensity, 2) no interference with other lines, and 3) no influence by predissociation. They are shown in Table 1, in which $Q1$, for example, means Q branch and $J' = J'' = 1$.

In the preceding part, it is shown that the theoretical spectra of Fulcher-α band are calculated as a function of three temperatures. However, the solution space is so wide that it is difficult to find a single set of the best-fit temperatures. There can be several local optimums to reproduce fairly the experimental data. In this work, the method to avoid such difficulty is proposed. When we can guess the rotational and vibrational temperatures with some accuracy, the true solution will be found by searching narrower space around them than in the case without guessing. Therefore, searching near the guessed temperatures enables us to identify the true temperatures more easily and more accurately. We call the method preprocessed line intensity fitting, which is explained in detail in the following part.

D. Preprocessing

The essential part of the preprocessed line intensity fitting method is how to guess the rotational and the vibrational temperatures. Considering that the temperatures at Fulcher upper state can be easily obtained by the Boltzmann plot technique, we guess the temperatures at the ground state by relating them to those at Fulcher upper state.

When we estimate the excitation rate coefficient, we assume that the rotational quantum number is unchanged in the transition. That is, Boltzmann distributions at the ground state and at Fulcher upper state are assumed to have the same shape for the variable J and J' when the values of v and v' are the same. We call it the similarity of Boltzmann distribution. Boltzmann distributions are shown as follows:

$$N_{v,J} \propto (2J+1) g_J \exp\left(-\frac{F(v,J)}{kT_{\mathrm{rot}}} - \frac{G(v)}{kT_{\mathrm{vib}}}\right) \tag{10}$$

$$N_{v',J'} \propto (2J'+1) g_{J'} \exp\left(-\frac{F(v',J')}{kT'_{\mathrm{rot}}} - \frac{G(v')}{kT'_{\mathrm{vib}}}\right) \tag{11}$$

Assuming the similarity of Boltzmann distribution, we obtain

$$\frac{F(v,J)}{T_{\mathrm{rot,guess}}} = \frac{F(v,J')}{T'_{\mathrm{rot}}} \tag{12}$$

From Eqs. (6) and (8), neglecting the second terms of them, the following relation is derived:

$$\frac{B_e}{T_{\mathrm{rot,guess}}} \simeq \frac{B'_e}{T'_{\mathrm{rot}}} \tag{13}$$

The error made in approximating Eq. (12) by Eq. (13) is within 2% in this case.

Likewise about the vibrational temperature, we assume the similarity of Boltzmann distribution. Letting the values of J and J' the same and fixed, and neglecting the second term of Eq. (7), we obtain a similar relation for T_{vib} such as

$$\frac{\omega_e}{T_{\mathrm{vib,guess}}} = \frac{\omega'_e}{T'_{\mathrm{vib}}} \tag{14}$$

The error made in neglecting the second term of Eq. (7) is within 7% in this case.

By Eqs. (13) and (14), temperatures at the ground state (denoted by no primes) are related to those at Fulcher upper state (denoted by single prime). When the latters are obtained, the formers are predicted from Eqs. (13) and (14).

Temperatures at Fulcher upper state are obtained by well-known Boltzmann plot method. In the case of the rotational temperature, 1) fixing the values of v' and v'', 2) neglecting the coupling of vibration and rotation, 3) substituting Eq. (11) to Eq. (1), and 4) taking the logarithm of both sides, we obtain

$$\log\left(\frac{I^{J'}_{J''}}{\nu^{J'}_{J''} A^{J'}_{J''} (2J'+1) g_{J'}}\right) = -\frac{F(J')}{kT'_{\mathrm{rot}}} + \mathrm{const} \tag{15}$$

By plotting the left side of Eq. (15) against $F(J')$, the rotational temperature of Fulcher upper state can be calculated from the slope of the plot. In this work, the rotational temperatures are separately calculated for $(v', v'') = (0,0), (1,1)$, and $(2,2)$. The averaged value of three cases is regarded as the rotational temperature of Fulcher upper state. The variation from the averaged value is within $\pm 30\%$ in our experiment.

Likewise in the case of vibrational temperature, fixing the values of J' and J'', we obtain the relation

$$\log\left(\frac{I^{v'}_{v''}}{\nu^{v'}_{v''} A^{v'}_{v''}}\right) = -\frac{G(v')}{kT'_{\mathrm{vib}}} + \mathrm{const} \tag{16}$$

The vibrational temperatures are separately calculated in the cases that $(J', J'') = (1,1)$, $(2,2)$, and $(3,3)$, and the averaged value is regarded as the vibrational temperature of Fulcher upper state. The variation from the averaged value is $\pm 25\%$ in our experiment.

Then, using Eqs. (13) and (14), the rotational and vibrational temperatures of the ground state can be guessed. In the intensity fitting, the true rotational and vibrational temperatures are expected to be near those estimates. The validity of this guessing process is evaluated in Sec. V.C.

The method to determine hydrogen plasma temperatures using Fulcher-α band spectra is summarized in Fig. 2. First, the rotational and vibrational temperatures at Fulcher upper state are obtained by Boltzmann plot method. Next, the rotational and vibrational temperatures at the ground state are guessed by the similarity of Boltzmann distribution. Then the true rotational, vibrational, and electron temperatures are obtained by the line intensity fitting.

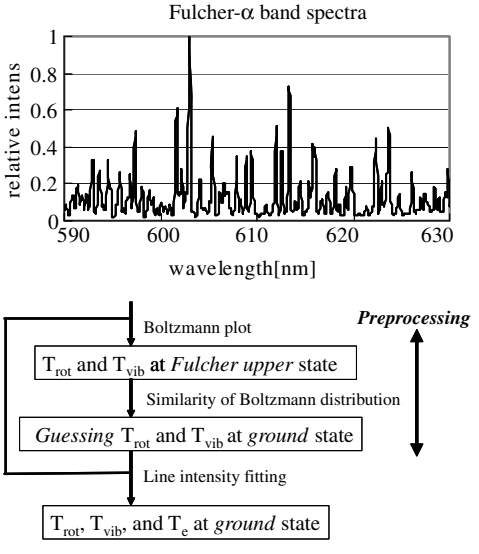

Fig. 2 Flow chart of preprocessed line intensity fitting.

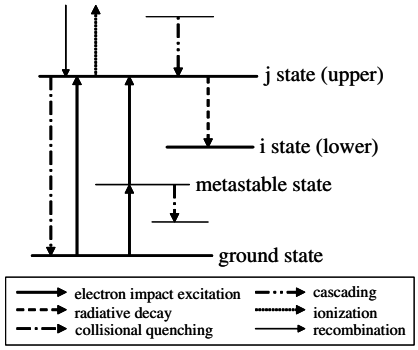

Fig. 3 Transition processes considered in actinometry.

III. Actinometry

For the measurement of the chemical composition, we use actinometry, which determines the degree of dissociation in plasma by seeding it with a small amount of a noble gas. It is calculated from the intensity ratio of a line of the dissociated molecule to that of the admixed gas. Argon is usually admixed in the case of hydrogen plasma [10,11].

Balmer H_α line (656.3 nm) for the $n = 3 \rightarrow n = 2$ transition ($E_{\text{thre}} = 12.06$ eV) and Ar 750.4 nm line for the $2p_1 \rightarrow 1s_2$ transition ($E_{\text{thre}} = 13.05$ eV) are used. Transition processes of both atoms are shown in Fig. 3. As the excitation and deexcitation paths, 1) direct electron impact excitation, 2) dissociative electron impact excitation, and 3) radiative decay are considered in this study.

1) Direct electron impact excitation:

$$\mathrm{H} + \mathrm{e}^- \rightarrow \mathrm{H}^*(n=3) + \mathrm{e}^-; k_H$$

$$\mathrm{Ar} + \mathrm{e}^- \rightarrow \mathrm{Ar}^*(2p_1) + \mathrm{e}^-; k_{\mathrm{Ar}}$$

2) Dissociative electron impact excitation:

$$\mathrm{H}_2 + \mathrm{e}^- \rightarrow \mathrm{H} + \mathrm{H}^*(n=3) + \mathrm{e}^-; k_{H_2}$$

3) Radiative decay:

$$\mathrm{H}^*(n=3) \rightarrow \mathrm{H}^{**}(n=2) + h\nu_{ij}^H; A_{ij}^H$$

$$\mathrm{Ar}^*(2p_1) \rightarrow \mathrm{Ar}^{**}(1s_2) + h\nu_{ij}^{\mathrm{Ar}}; A_{ij}^{\mathrm{Ar}}$$

k_H, k_{H_2}, and k_{Ar} are excitation rate coefficients defined as

$$k_i = \int_{E_{\text{thre},i}}^{\infty} \sigma_i \sqrt{\frac{2E}{m_e}} f(E)\, \mathrm{d}E \qquad (i = \mathrm{H}, \mathrm{H}_2, \mathrm{Ar}) \tag{17}$$

where σ_i and $f(E)$ are the excitation cross section and electron energy distribution function, respectively. The distribution function is assumed to be Maxwellian, which is a function of electron temperature obtained by the preprocessed line intensity fitting. Other paths shown in Fig. 3, such as collisional quenching, stepwise excitation, cascading, ionization, and recombination, are neglected. The possible error by this assumption is evaluated in Sec. V.D.4.

Assuming the steady state, the population balance of H and Ar yields

$$I_{H^*,ij} = \frac{h\nu_{ij}^H A_{ij}^H n_e}{\sum_m A_{im}^H} (k_H N_H + k_{H_2} N_{H_2}) \tag{18}$$

$$I_{\mathrm{Ar}^*,ij} = \frac{h\nu_{ij}^{\mathrm{Ar}} A_{ij}^{\mathrm{Ar}} n_e}{\sum_m A_{im}^{\mathrm{Ar}}} k_{\mathrm{Ar}} N_{\mathrm{Ar}} \tag{19}$$

where the summation in Eqs. (18) and (19) means the consideration of the possible lower states m, to which H or Ar atom can deexcite from the upper state i by radiative decay. N_H/N_{H_2} is described in terms of $I_{H^*}/I_{\mathrm{Ar}^*}$ and N_{Ar}/N_{H2} as follows:

$$\frac{N_H}{N_{H_2}} = \frac{I_{H^*}}{I_{\mathrm{Ar}^*}} \frac{1}{K_{H,\mathrm{Ar}}} \frac{k_{\mathrm{Ar}}}{k_H} \frac{N_{\mathrm{Ar}}}{N_{H_2}} - \frac{k_{H_2}}{k_H}, \qquad K_{H,\mathrm{Ar}} = \frac{\nu_{ij}^H A_{ij}^H \left(\sum_m A_{im}^H\right)^{-1}}{\nu_{ij}^{\mathrm{Ar}} A_{ij}^{\mathrm{Ar}} \left(\sum_m A_{im}^{\mathrm{Ar}}\right)^{-1}} \tag{20}$$

If the number of the ions is negligible, the degree of dissociation is finally given by

$$\alpha = \frac{N_H/N_{H_2}}{(N_H/N_{H_2}) + 2} \tag{21}$$

The data of the excitation cross sections σ_H, σ_{H_2}, and σ_{Ar} are necessary to calculate the excitation rate coefficient by Eq. (17). Many theoretical or experimental researches have been made on it so far. Among them we should use the cross section data satisfying the following conditions for the accurate calculation of the rate coefficient:

1) A sufficiently large number of data are given near the threshold energy.

2) The influences of other processes such as cascading and stepwise excitation are eliminated in obtaining their data.

Regarding the direct electron impact excitation cross section of H_α line, σ_H, data by Mansky and Flannery [12], Mahan et al. [13], and Lavrov and Pipa [14] are used, and they show a fairly good agreement. Regarding the dissociative electron impact excitation cross section of H_α line, σ_{H_2}, the data by Lavrov and Pipa [14] are used because it has a large number of data near the threshold energy.

Regarding the excitation cross section of Ar 750.4 nm line, σ_{Ar}, there are also many researches. However, Gathen and Döbele [11] pointed out that several data are overestimated because of the inability to exclude the cascading process and that only the results by Chutjian and Cartwright [15] and Bogdanova and Yurgenson [16] do not contain the influence of cascading. However, their data are not appropriate to calculate the rate coefficients owing to the lack of the measurement points near the threshold energy. Then, we use the data set used by Katsch et al. [17], because it has many data near the threshold energy and its values are close to those by Chutjian and Cartwright [15] and Bogdanova and Yurgenson [16].

IV. Experimental Setup

A. ICP Facility

The aforementioned spectroscopic diagnostics of thermochemical nonequilibrium hydrogen plasma has been applied to our ICP wind tunnel. This wind tunnel aims for the aerocapture simulator by the high-altitude flight of the low-ballistic-coefficient spacecraft [18]. As a fundamental research before its test, we must determine the freestream conditions of this wind tunnel. The radio-frequency (RF) inductive heating is used to produce nonequilibrium plasma. Although the ICP flow operated at relatively high pressure (1–100 kPa) is known to be nearly in thermal equilibrium [19,20], the flow is expected to be in thermochemical nonequilibrium because of the insufficient collisions when ICP is produced at lower pressure.

The schematic view of our ICP facility is shown in Fig. 4. The wall of the flow channel is made from quartz and its shape is shown in Fig. 5. The use of a transparent tube enables us to observe the whole plasma flow in the wind tunnel and to measure the spatial variations of the nonequilibrium quantities. The transmissivity of the quartz is uniformly 0.925 in the wavelength range used in this experiment. The nozzle throat diameter and the nozzle exit diameter are 10 mm and 30 mm, respectively. A water-cooled coil is surrounding the cylindrical section of the tube by four turns, and a RF power supply with its frequency of 13.56 MHz and maximum output power 2 kW is connected to a matching network, which vanishes the power reflected from the plasma. The test gas is injected from the two ports in the way of colliding jets. The test gas is hydrogen admixed with a small amount of argon.

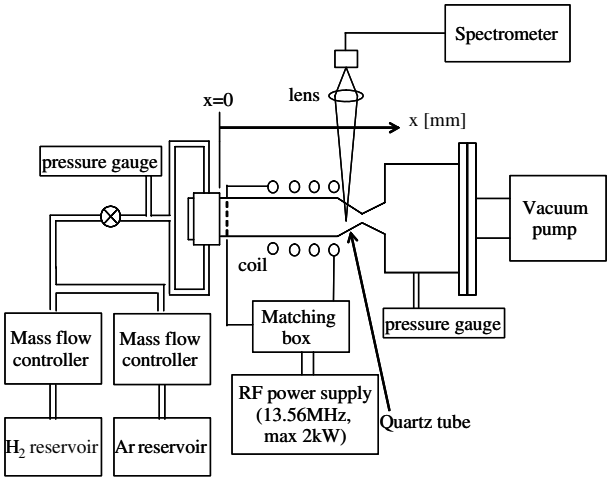

Fig. 4 Schematic view of ICP wind tunnel.

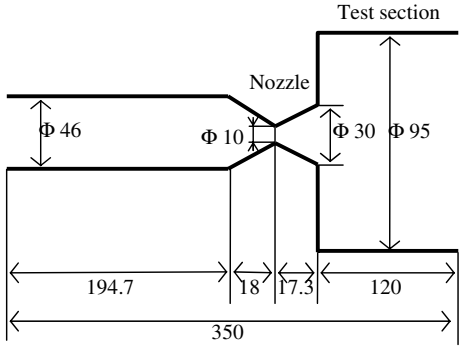

Fig. 5 Shape of quartz tube used in ICP wind tunnel (unit: mm).

B. Optical System

The optical system and the coordinate are also shown in Fig. 4. The measurement point is determined by the lens system installed in front of the spectrometer. The emission focused by the lens is put into the spectrometer (Hamamatsu, PMA-50) through the optical fiber. The resolution of the spectral measurement is 0.08 nm, and the wavelength width that can be observed at a single data sampling is 61.5 nm. The measurement data are obtained by averaging 10 samples. The exposure time is 800 ms in the preprocessed line intensity fitting and 40 ms in the actinometry, respectively.

V. Results and Discussion

A. Experimental Condition

The test gas is hydrogen admixed with argon. The mass flow rate of hydrogen is changed such as 1, 1.5, 2 SLM (1 SLM= 1.40×10^{-6} kg/s). The mass flow rate of argon is set as 0.1 SLM (1 SLM = 2.77×10^{-5} kg/s) to satisfy the following conditions:

1) It is large enough to give the enough intensity of 750.4 nm line used in the actinometry.

2) It is small enough not to have influence on the spectroscopic measurement of Fulcher-α band, because the wavelength domain of several argon line spectra overlaps that of Fulcher-α band.

Therefore, the ratio of hydrogen and argon appropriate for the spectrometry is limited. In our experiments, by comparing to the case that no argon is admixed, we have confirmed that Fulcher-α spectra are not disturbed by the presence of Ar. The admixed argon does not have influence on the spectroscopic measurements of Fulcher-α band and the determination of the temperatures. In addition, this mass flow rate of argon gives the sufficient emission intensity of Ar 750.4 nm line for the actinometry.

The input power is constantly 500 W. The specific enthalpy of the gas is expected to increase with the decrease in the mass flow rate because the input power is constant in the present study. The stagnation pressure is about 100 Pa. Knudsen number is 0.0–0.1 in the whole flow channel when the characteristic length is the tube diameter. The present ICP flow is in the transitional or rarefied flow regimes. Figure 6 shows the emission of hydrogen plasma in the case that the mass flow rate of H_2 is 1 SLM.

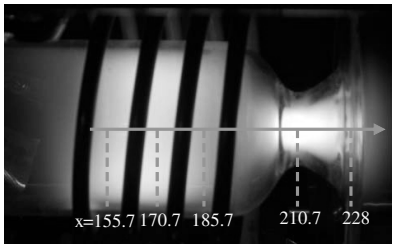

Fig. 6 Emission of hydrogen plasma.

Measurement points are set along the centerline of the quartz tube. The spectrometer detects the integral of all the emission on the line of observation. The temperatures, the degree of dissociation, and so on are the mean values over the tube diameter at the position on the x axis, which is indicated in Fig. 6. However, this mean value is thought to be almost equal to the value at the centerline. We have confirmed the uniformity of plasma temperatures at $x = 170.7$ mm by conducting the Abel inversion. The temperatures are almost uniform in the region where the radius is from 0 to 20 mm. The tube radius at the position is 23 mm.

Our method to diagnose the hydrogen plasma and to determine the freestream condition of our ICP wind tunnel is as follows: The rotational, vibrational, and electron temperatures are obtained by the preprocessed line intensity fitting. Then, the degree of dissociation is obtained by the actinometry. Finally, the total enthalpy of dissociating hydrogen gas flow is calculated by using those three temperatures and the degree of dissociation.

B. Plasma Temperatures and Degree of Dissociation

Figures 7–9 show the rotational, the vibrational, and the electron temperature profiles along the tube axis at the various mass flow rates of hydrogen. The method to determine the error bar in the figures is explained in Sec. V.C. In each case T_e is the highest. T_{vib} is the second highest, and T_{rot} is the lowest. The present ICP flow is in strong thermal nonequilibrium, which is caused because the collisions under our experimental conditions are not sufficient enough to lead the thermal equilibrium. It is of much interest that T_e is increasing from the nozzle inlet to the nozzle throat (190 mm $< x <$ 210 mm), while T_{vib} is almost constant, and T_{rot} is gradually decreasing. This is expected to be because the induced current is confined in the narrower region toward the nozzle throat and the current density gets larger. However, the present work is not enough to clarify this interesting phenomenon. It is our future work. These experimental results indicate the following:

1) The electron is significantly heated in the nozzle upstream region (190 $< x <$ 210 mm).

2) The vibrational–translational relaxation is almost frozen in the flow.

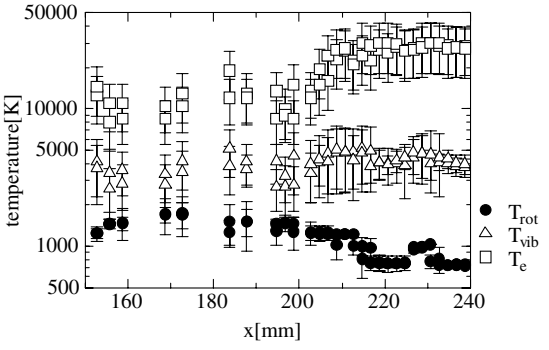

Fig. 7 Plasma temperatures at H_2 1 SLM, Ar 0.1 SLM.

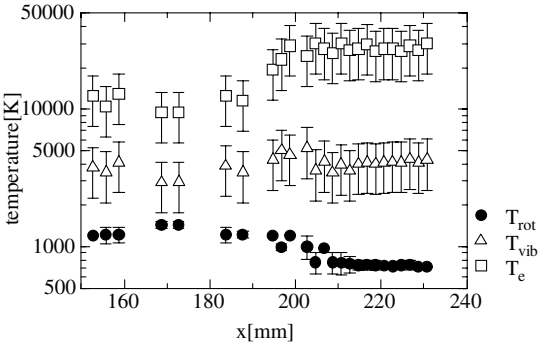

Fig. 8 Plasma temperatures at H_2 1.5 SLM, Ar 0.1 SLM.

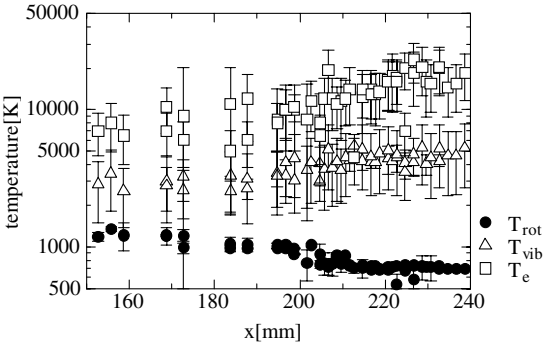

Fig. 9 Plasma temperatures at H_2 2 SLM, Ar 0.1 SLM.

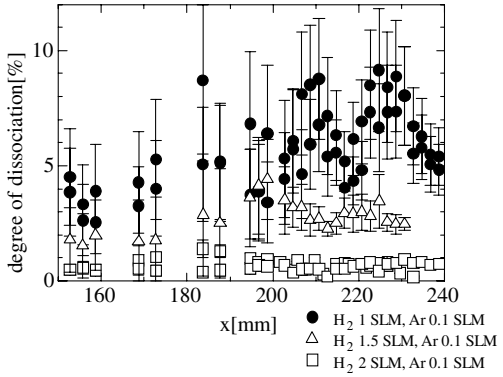

Fig. 10 Degree of dissociation.

3) Because of very quick rotational–translational relaxation, the translational and rotational modes are expected to be in equilibrium and their energies are converted into the kinetic energy of the flow in the nozzle region.

The profiles of the degree of dissociation are shown in Fig. 10. It shows that the degree of dissociation increases significantly when the mass flow rate decreases.

C. Improvement of Spectral Fitting by Preprocessing

The advantage of guessing the rotational and the vibrational temperature is shown here. We consider the situation where the spectra shown in Fig. 11 are measured. Without guessing them, there are several local optimums in the solution space, such as cases a, b, c, and d in Table 2. However, we can determine the true temperatures by preprocessing. In this case, $T_{rot,guess}$ is 1100 K and $T_{vib,guess}$ is 2900 K. $T_{vib,guess}$ is higher by 1800 K than $T_{rot,guess}$. Therefore, searching the domain where T_{vib} is higher than T_{rot} and specifying the closest values to the guessed values, case b is chosen as the best fitting. In our experiments, T_{vib} is not away from the guessed value, whereas T_{rot} is about twice larger than the guessed value. The rotational and vibrational temperatures at Fulcher upper state are

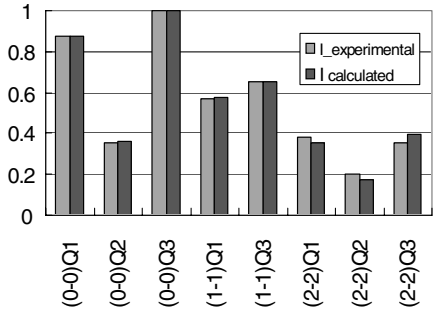

Fig. 11 Example of the fitting results.

550 K and 1600 K, respectively. Therefore, our experimental results indicate that the rotational and vibrational temperatures at the ground state are not equal to those at the excited states. An example of the fitting results is shown in Fig. 11. The experimental and calculated spectra show a very good agreement.

D. Error Evaluation

1. Error Evaluation in Preprocessed Line Intensity Fitting

In the error of the preprocessed line intensity fitting, we distinguish the measurement and fitting errors from the theoretical uncertainty that stems from the assumptions in the method. The error bar of the experimental results shown in Sec. V.B is written by considering only the measurement and fitting errors. Theoretical uncertainty cannot be assessed quantitatively, though the total enthalpy obtained in Sec. V.E shows a reasonable tendency and it does not seem significant.

The peak intensity detected by the spectrometer is expected to depend on the resolution in wavelength. To evaluate such uncertainty, we use the (0-0)$Q3$ line (603.19 nm), and change the center wavelength of the measurement by 0.01 nm around it. As a result, the variation of the peak intensity is within 5%, and the spectrometer can detect its peak intensity. With respect to the fitting error, the difference between the measured and calculated intensity is estimated about 5% on average according to Fig. 11. As a result, the errors of rotational, vibrational, and electron temperatures calculated from those intensity errors are about $\pm 10\%$, $\pm 30\%$, and $\pm 40\%$ on average, respectively.

2. Evaluation for Assumption of Corona Equilibrium in Preprocessed Line Intensity Fitting

In the present preprocessed line intensity fitting, corona equilibrium is assumed. Compared with the exact but tough solution by master equations that request us to prepare the rate coefficients for all the transitions of hydrogen molecule, the solution by corona equilibrium is easy to use owing to its simplicity. Generally, corona equilibrium is valid in the case of the plasma with low electron number density and high electron temperature, like solar corona. ICP studied in this work is expected to be close to this situation.

Because the stepwise excitation, the dissociation, and the recombination are considered to occur rarely, only the deexcitation by collisional quenching is investigated here. The radiative lifetime at $d^3\Pi_u$ state is around 30 ns [21,22]. On the other hand, the mean collision time is calculated to be around 300 ns under our experimental conditions by using the cross section value obtained by Marechal et al. [21]. Therefore, the radiation occurs much more frequently than the collisional quenching, which supports the assumption of corona equilibrium.

Table 2 Effect of guessing

Case	T_{rot}, K	T_{vib}, K	T_e, K
a	1700	18,300	150,000
b	2100	3,800	29,500
c	3700	2,600	18,500
d	4600	12,000	150,000

3. Error Evaluation in Actinometry

From Eq. (21), the relative error for α is almost the same as that for N_H/N_{H_2}:

$$\frac{\delta\alpha}{\alpha} = \frac{1}{\alpha}\left|\frac{\partial\alpha}{\partial(N_H/N_{H_2})}\right|\delta\left(\frac{N_H}{N_{H_2}}\right) = \frac{2}{(N_H/N_{H_2})+2}\frac{\delta(N_H/N_{H_2})}{N_H/N_{H_2}} \approx \frac{\delta(N_H/N_{H_2})}{N_H/N_{H_2}} \tag{22}$$

where N_H/N_{H_2} is less than 0.1 in our experiments. The error of each term in Eq. (20) is estimated next.

The errors of I_{H^*} and I_{Ar^*} are obtained by their temporal variations. The errors of k_{Ar}, k_H, and k_{H_2} are obtained by calculating the dependency on the electron temperature and the cross section data. About N_{Ar}/N_{H_2}, the mass flow rates of both hydrogen and argon are measured at the inlet. The flow velocities of hydrogen and argon are assumed to be the same, and the ratio is assumed to be constant everywhere in the flow. However, actually, the dissociation reaction of H_2 occurs; therefore the number density of H_2 is $(1-\alpha)N_{H_2,\text{inlet}}$. Considering the degree of dissociation obtained in the experiment, the error is at most 10%. As a result, the error of the degree of dissociation is about $\pm 30\%$ on average.

4. Evaluations of Other Transition Processes in Actinometry

In the present actinometry, the transition processes other than the electron impact excitation and the radiation are neglected. To consider the accuracy of the preceding assumption, we evaluate the effects of the stepwise excitation, the collisional quenching, the ionization, and the recombination shown in Fig. 3 for our typical experimental condition. We do not evaluate the effect of the cascading because no data are available for the calculation of the cascading rate coefficient.

The stepwise excitation through the metastable states exists in both hydrogen and argon. The quenching and electron impact excitation coefficients at the metastable state in both gases are shown by Gicquel et al. [23]. Then their frequencies are calculated for the typical experimental conditions. For hydrogen, the quenching frequency is 6.6×10^6 s^{-1}, and the electron impact excitation frequency is 1.3×10^1 s^{-1}. For argon, the quenching frequency is 7.4×10^5 s^{-1}, and the electron impact excitation frequency is 1.3×10^3 s^{-1}. For both gases, the quenching occurs at the metastable state much more frequently than the electron impact excitation. Therefore, the stepwise excitation for both gases is negligible.

Particles in the upper states (denoted by j state in Fig. 3) deexcite by the radiative decay and by the collisional quenching. The quenching rate coefficients of H ($n=3$) are investigated separately by Bittner et al. [24] and Preppernau et al. [25] and their values are in good agreement. With respect to quenching rate coefficients of Ar ($2p_1$) state, the values shown by Francis et al. [26] are used. For the typical experimental condition, the quenching frequency of hydrogen is 7.9×10^6 s^{-1}, and the sum of the transition probabilities from the upper electronic state is 8.7×10^7 s^{-1}. Consequently, the quenching of H ($n=3$) should be taken into account by replacing $\sum_j A_{ij}^H$ in Eq. (19) by $\sum_j A_{ij}^H + \nu_{\text{quench}}$. The quenching of H has an influence on the intensity of hydrogen line by about 10%. For argon, the quenching frequency is 1.2×10^5 s^{-1}, and the sum of the transition probabilities is 4.5×10^7 s^{-1}. Therefore, the quenching of Ar is negligible.

The ionization energy of H is 13.6 eV, which is much larger than the dissociation energy of H_2, 4.4 eV. The degree of dissociation in the present study is at most 10%. The degree of ionization of H is expected to be much smaller, and the recombination reaction can be also regarded as negligible. With respect to the ionization of argon, there are no Ar^+ lines observed in our experiment. Therefore, it can be also neglected.

E. Calculation of Enthalpy

The total enthalpy of hydrogen plasma flow at the nozzle exit is composed of the internal energy calculated by the temperature of each energy mode, the kinetic energy, and the energy consumed for the chemical reaction. Hydrogen plasma consists of H_2, H, H^+, and e^-; however, H^+, and e^- can be neglected because of the extremely low degree of ionization. The reference temperature of internal energy is 290 K. Thus the enthalpy of the gas mixture of hydrogen molecule and atom, H_{mix} can be given by

$$h_{H_2} = c_{p,H_2,\text{tra}}(T_{\text{tra}}-290) + \int_{290}^{T_{\text{rot}}} c_{v,H_2,\text{rot}}\,\mathrm{d}T + \int_{290}^{T_{\text{vib}}} c_{v,H_2,\text{vib}}\,\mathrm{d}T + \int_{290}^{T_{\text{ele}}} c_{v,H_2,\text{ele}}\,\mathrm{d}T + h_{H_2,\text{kinetic}} + h_{\text{chem}} \tag{23}$$

$$h_H = c_{p,H,\text{tra}}(T_{\text{tra}}-290) + \int_{290}^{T_{\text{ele}}} c_{v,H,\text{ele}}\,\mathrm{d}T + h_{H,\text{kinetic}} \tag{24}$$

$$H_{\text{mix}(H_2,H)} = Y_{H_2}h_{H_2} + Y_H h_H \tag{25}$$

The method to estimate each component is shown as follows:

1) Translational mode of H_2 and H: When the equilibrium between the translational and the rotational modes is assumed, the translational temperature is equal to its rotational temperature. The specific heat at constant pressure of the translational mode is $5R_{H_2}/2$ or $5R_H/2$.

2) Rotational mode of H_2: Rotational temperature measured in our experiments is much higher than the characteristic temperature of the rotational excitation for H_2, 85.4 K. Because the rotational mode is expected to be fully excited, the specific heat of the rotational mode is equal to R_{H_2}.

3) Vibrational mode of H_2: Assuming the harmonic oscillator model, the specific heat of the vibrational mode is described as follows:

$$c_{v,\text{vib}} = R_{H_2}\left(\frac{\theta_{\text{vib}}}{T_{\text{vib}}}\right)^2 \frac{\exp(\theta_{\text{vib}}/T_{\text{vib}})}{[\exp(\theta_{\text{vib}}/T_{\text{vib}})-1]^2} \tag{26}$$

where θ_{vib} is the characteristic temperature of the vibrational excitation for H_2, 6159 K.

4) Electronic mode of H_2 and H: The specific heat of the electronic mode is calculated by the following equations:

$$c_{v,\text{el}} = R\left(\frac{T_{\text{el}}}{k}\right)^2\left[\frac{D_3}{D_1} - \left(\frac{D_2}{D_1}\right)^2\right] \tag{27}$$

$$D_1 = \sum_i g_i \exp\left(-\frac{E_i}{kT_{\text{el}}}\right), \qquad D_2 = \sum_i g_i E_i \exp\left(-\frac{E_i}{kT_{\text{el}}}\right) \qquad D_3 = \sum_i g_i E_i^2 \exp\left(-\frac{E_i}{kT_{\text{el}}}\right) \tag{28}$$

where g_i and E_i are the degeneracy and the electronic energy of the ith state, respectively. The values are given by Bose [27]. The summation is done up to the fourth-lowest energy state.

The typical electronic excitation temperature of H atom obtained by Boltzmann plot of Balmer lines is 2000–4000 K. When we assume the excitation temperature of H_2 is equal to that of H, the calculated electronic excitation energy is less than 0.01 MJ/kg for both H_2 and H. Therefore, the contribution of the electronic mode to H_{mix} is negligible.

5) Kinetic energy of H_2 and H: Flow velocity cannot be measured directly by the present method. However, the kinetic energy is expected to be the same as the decrease in the translational and the rotational energies if the following conditions are assumed:

a) The flow velocity near the coil is negligible because it is small enough compared with that at the nozzle exit.

b) Only the translational and the rotational energies are converted into the kinetic energy of the flow. The other modes are frozen in the nozzle.

c) The translational and rotational modes are in equilibrium.

d) The velocity of H_2 is equal to that of H.

Table 3 Composition of the total specific enthalpy

	H_2 mass flow rate, SLM		
	1	1.5	2
Deg. of dissociation, %	7.3	2.6	0.45
Trans. energy, H_2, MJ/kg	4.6	4.4	2.5
Rot. energy, H_2, MJ/kg	1.9	1.7	1
Vib. energy, H_2, MJ/kg	7.9	7.9	8.4
Ele. energy, H_2, MJ/kg	<0.01	<0.01	<0.01
Trans. energy, H, MJ/kg	9.2	8.8	5.0
Ele. energy, H, MJ/kg	<0.01	<0.01	<0.01
Chemical, MJ/kg	15.5	5.5	1.0
Kinetic energy, MJ/kg	6.0	4.7	4.6
Flow velocity, m/s	4000	3300	3300
Total enthalpy, MJ/kg	34.4	23.9	17.4

6) Chemical reaction: Only the energy consumed for the dissociation reaction of hydrogen molecule is taken into account. It is calculated from the degree of dissociation.

The composition of H_{mix} can be calculated as shown in Table 3. The error of the total enthalpy is evaluated as about $\pm 40\%$ by taking the summation component by component. The fact that the total enthalpy is almost inversely proportional to the mass flow rate of H_2 seems quite reasonable under the constant input power condition.

VI. Conclusions

A method to diagnose thermochemical nonequilibrium hydrogen plasma flow nonintrusively by emission spectroscopy has been developed. The rotational, vibrational, and electron temperatures have been obtained by the preprocessed line intensity fitting of Fulcher-α band, and the degree of dissociation by the actinometry. In the preprocessed line intensity fitting, we guess the rotational and vibrational temperatures before the intensity fitting to make the searching domain smaller. As a result, our fitting method has made it possible to identify those three temperatures more easily.

Then our method has been applied to our ICP wind tunnel. From the experimental results, we have determined the freestream conditions of the wind tunnel. It is experimentally found that the rotational and vibrational temperatures at the ground state are different from those at the excited states. The obtained total enthalpy, which is composed of the internal energy, kinetic energy, and chemical energy, shows a reasonable tendency to be almost inversely proportional to the mass flow rate under the condition of fixed input power. The possible error in the temperatures, the degree of dissociation, and the total enthalpy is evaluated in the component-by-component manner.

Acknowledgments

This work is supported by Grant-in-Aid for Scientific Research No. 17360408 of Japan Society for the Promotion of Science. The primary author is supported by Research Fellowships of the Japan Society for the Promotion of Science for Young Scientists.

References

[1] Fantz, U., and Heger, B., "Spectroscopic Diagnostics of the Vibrational Population in Ground State of H_2 and D_2 Molecules," *Plasma Physics and Controlled Fusion*, Vol. 40, No. 12, 1998, pp. 2023–2032.

[2] Surrey, E., and Crowley, B., "Spectroscopic Measurement of Gas Temperature in the Neutralizer of JET Neutral Beam Injection System," *Plasma Physics and Controlled Fusion*, Vol. 45, No. 7, 2003, pp. 1209–1226.

[3] Tomasini, L., Rousseau, A., Gousset, G., and Leprince, P., "Spectroscopic Temperature Measurements in a H_2 Microwave Discharge," *Journal of Physics D: Applied Physics*, Vol. 29, No. 4, 1996, pp. 1006–1013.

[4] Lavrov, B. P., "Determination of the Gas Temperature of a Low-Pressure Plasma from the Intensities of the H_2 and D_2 Molecuar Bands," *Optics and Spectroscopy (USSR)*, Vol. 48, No. 4, 1980, pp. 375–380.

[5] Herzberg, G., *Molecular Spectra and Molecular Structure 1: Spectra of Diatomic Molecules*, RE Krieger Publishing Company, Malabar, FL, 1989.

[6] Ginsburg, N., and Dieke, G. H., "Intensity Measurements in the Molecular Spectrum of Hydrogen," *Physical Review*, Vol. 59, No. 8, 1941, pp. 632–644.

[7] Spindler, J. R., "Franck-Condon Factors for Band Systems of Molecular Hydrogen 1," *Journal of Quantitative Spectroscopy and Radiative Transfer*, Vol. 9, No. 5, 1969, pp. 597–626.

[8] Baltayan, P., and Nedelec, O., "Relative Intensities and Polarizations in H Rotational Lines Excited by Electron Impact," *Journal de Physique*, Vol. 36, No. 2, 1975, pp. 125–133.

[9] Gans, T., Gathen, V. S., and Döbele, H. F., "Time Dependence of Rotational State Populations of Excited Hydrogen Molecules in an RF Excited Plasma Reactor," *Plasma Sources Science and Technology* , Vol. 10, No. 1, 2001, pp. 17–23.

[10] St-Onge, L., and Moisan, M., "Hydrogen Atom Yield in RF and Microwave Hydrogen Discharges," *Plasma Chemistry and Plasma Processing*, Vol. 14, No. 2, 1994, pp. 87–116.

[11] Gathen, V. S., and Döbele, H. F., "Critical Comparison of Emission Spectroscopic Determination of Dissociation in Hydrogen RF Discharges," *Plasma Chemistry and Plasma Processing*, Vol. 16, No. 4, 1996, pp. 461–486.

[12] Mansky, E. J., and Flannery, M. R., "The Multichannel Eikonal Theory of Electron-Hydrogen Collisions: 1. Excitation of H(1s)," *Journal of Physics B: Atomic, Molecular and Optical Physics*, Vol. 23, No. 24, 1990, pp. 4549–4572.

[13] Mahan, A. H., Gallagher, A., and Smith, S. J., "Electron Impact Excitation of the 3S, 3P, and 3D States of H," *Physical Review A*, Vol. 13, No. 1, 1976, pp. 156–166.

[14] Lavrov, B. P., and Pipa, A. V., "Account of the Fine Structure of Hydrogen Atom Levels in the Effective Emission Cross Sections of Balmer Lines Excited by Electron Impact in Gases and Plasma," *Optics and Spectroscopy (USSR)*, Vol. 92, No. 5, 2002, pp. 647–657.

[15] Chutjian, A., and Cartwright, D. C., "Electron-Impact Excitation of Electronic States in Argon at Incident Energies Between 16 and 100 eV," *Physical Review A*, Vol. 23, No. 5, 1981, pp. 2178–2193.

[16] Bogdanova, I. P., and Yurgenson, S. V., "Cross Sections for Direct Electronic Excitation of Atomic Levels: Measurements Using a Pulsed Electron Beam and Time-Base Scanning of Radiation 2: Argon, $3p^5 4p$ Level," *Optics and Spectroscopy (USSR)*, Vol. 62, No. 2, 1987, pp. 281–282.

[17] Katsch, H. M., Tewes, A., Quandt, E., Goehlich, A., Kawetzki, T., and Döbele, H. F., "Detection of Atomic Oxygen: Improvement of Actinometry and Comparison with Laser Spectroscopy," *Journal of Applied Physics*, Vol. 88, No. 11, 2000, pp. 6232–6238.

[18] Nakamura, K., and Suzuki, K., "Aerothermodynamic Analysis on Low-Ballistic-Coefficient Aerocapture Vehicle with Membrane Decelerator," IAC Paper 05-E2.2.03, 2005.

[19] Fujita, K., Mizuno, M., Ishida, K., Ito, T., and Kurotaki, T., "Comprehensive Spectroscopic Measurements in ICP-Heated Wind Tunnel Plasmas," *Proceedings of the 24th International Symposium on Space Technology and Science*, ISTS Paper 2004-e-32, Miyazaki, Japan, 2004.

[20] Abeele, D. V., and Degrez, G., "Efficient Computational Model for Inductive Plasma Flows," *AIAA Journal*, Vol. 38, No. 2, 2000, pp. 234–242.

[21] Marechal, M. A., Lost, R., and Lombardi, M., "Lifetimes, g Factors, and Collision Cross Sections of Hydrogen Molecules in the $(1s3p)^3\Pi_u$ Level," *Physical Review A*, Vol. 5, No. 2, 1972, pp. 732–740.

[22] Kiyoshima, T., and Sato, H., "Perturbation Effects on Lifetimes of $d^3\Pi_u$ States in H_2 and D_2," *Physical Review A*, Vol. 48, No. 6, 1993, pp. 4771–4774.

[23] Gicquel, A., Chenevier, M., Hassouni, K., Tserepi, A., and Dubus, M., "Validation of Actinometry for Estimating Relative Hydrogen Atom Densities and Electron Energy Evolution in Plasma Assisted Diamond Deposition Reactors," *Journal of Applied Physics*, Vol. 83, No. 12, 1998, pp. 7504–7521.

[24] Bittner, J., Kohse-Höinghaus, K., Meier, U., and Just, T., "Quenching of Two-Photon-Excited H(3s,3d) and O($3p\ ^3P_{2,1,0}$) atoms by Rare Gases and Small Molecules," *Chemical Physics Letters*, Vol. 143, No. 6, 1988, pp. 571–576.

[25] Preppernau, B. L., Pearce, K., Tserepi, A., Wurzberg, E., and Miller, T. A., "Angular Momentum State Mixing and Quenching of $n = 3$ Atomic Hydrogen Fluorescence," *Chemical Physics*, Vol. 196, No. 2, 1995, pp. 371–381.

[26] Francis, A., Czarnetzki, U., and Döbele, H. F., "Quenching of the 750.4 nm Argon Actinometry Line by H and Several Hydrocarbon Molecules," *Applied Physics Letters*, Vol. 71, No. 26, 1997, pp. 3796–3798.

[27] Bose, T. K., *High Temperature Gas Dynamics: An Introduction for Physicists and Engineers*, Springer–Verlag, New York, 2004.